Title
Multiscale modeling of spatially variable water and energy balance processes

Permalink
https://escholarship.org/uc/item/0n10f7nw

Journal
Water Resources Research, 30(11)

ISSN
0043-1397

Authors
Famiglietti, JS
Wood, EF

Publication Date
2010-07-09

DOI
10.1029/94WR01498

Multiscale modeling of spatially variable water and energy balance processes

J. S. Famiglietti

Department of Geological Sciences, University of Texas at Austin

E. F. Wood

Water Resources Program, Department of Civil Engineering and Operations Research
Princeton University, Princeton, New Jersey

Abstract. This paper presents the model development component of a body of research which addresses aggregation and scaling in multiscale hydrological modeling. Water and energy balance models are developed at the local and catchment scales and at the macroscale by aggregating a simple soil-vegetation-atmosphere transfer scheme (SVATS) across scales in a topographic framework. A spatially distributed approach is followed to aggregate the SVATS to the catchment scale. A statistical-dynamical approach is utilized to simplify the large-scale modeling problem and to aggregate the SVATS to the macroscale. The resulting macroscale hydrological model is proposed for use as a land surface parameterization in atmospheric models. It differs greatly from the current generation of land surface parameterizations owing to its simplified representation of vertical process physics and its statistical representation of horizontally heterogeneous runoff and energy balance processes. The spatially distributed model formulation is explored to understand the role of spatial variability in determining areal-average fluxes and the dynamics of hydrological processes. The simpler macroscale formulation is analyzed to determine how it represents these important dynamics, with implications for the parameterization of runoff and energy balance processes in atmospheric models.

1. Introduction

The hydrologic cycle is a major component of the earth's climate system. It interacts with the other system components (the solid Earth, the oceans, and the atmosphere) over a wide range of spatial and temporal scales. This interaction affects a number of physical, chemical, and biological processes, including climate, weather, biogeochemical cycles, and ecosystem dynamics. However, the nature of these interactions, including their mechanisms and impacts, is poorly understood.

Studies of such coupled-system problems are often conducted using numerical atmospheric models. A number of studies with general circulation models (GCMs) and mesoscale atmospheric models have shown that the land component of the hydrologic cycle is particularly responsible for maintaining long-term climate and the temporal variability of weather and climate (see *Mintz* [1984], *Avissar and Verstraete* [1990], and *Wood* [1991] for reviews of these studies). However, a major acknowledged weakness in these atmospheric models is that the grid-scale (macroscale) parameterizations of land surface hydrology are often overly simplistic representations of complex, spatially variable processes of land-atmosphere interaction. Improving the reliability in macroscale hydrological models is a critical step toward understanding the relationship between the hydrologic cycle and the other components of the Earth system.

To develop more realistic parameterizations of land-hydrological processes, hydrologists require an improved understanding of the land surface water and energy balance over a range of increasing spatial scales. Gaining this understanding is not straightforward, because as the scale of the hydrologic modeling problem increases, the complexity of the problem increases as well. One of the major issues in developing larger-scale hydrological models is known as the aggregation problem, that is, What is the proper representation of macroscale hydrologic response given that the dynamics of hydrological processes occur over various spatial and temporal scales? The problem is compounded by the tremendous natural heterogeneity of the land surface. A second and related issue is the scale problem, that is, What is the relationship between spatial variability, scale, and the realistic description of hydrological processes? The aggregation and scale issues are related because the aggregation problem depends on the degree of spatial variability of hydrological processes and the scale of the modeling problem.

This paper presents the model development component of a body of research which addresses aggregation and scaling in multiscale hydrological modeling. Methodologies for aggregating process physics known at small scales to the catchment and macroscales are presented. Water and energy balance models at the local, catchment, and macroscales are described. In a second paper [*Famiglietti and Wood*, this issue] the models are applied at their appropriate scales at the site of the First International Satellite Land Surface Climatology Project (ISLSCP) Field Experiment (FIFE). A

third paper [*Famiglietti and Wood*, 1994] (hereinafter referred to as paper 3) explores the interrelationship between the aggregation and scale problems. The scales at which spatially variable hydrological processes must be represented explicitly, using a spatially distributed approach (explicit aggregation), or statistically, using a statistical-dynamical approach (statistical aggregation), are investigated. The existence of a threshold modeling scale, which marks the transition in modeling requirements, is investigated as well.

The remainder of this paper is organized as follows. In section 2, coupled water and energy balance models are presented at the local scale, catchment scale, and macroscale. A topographic framework, previously used to aggregate runoff processes to larger scales [*Beven and Kirkby*, 1979; *Beven*, 1986; *Sivapalan et al.*, 1987], is invoked to aggregate both runoff and energy balance processes to the catchment scale and macroscale. In section 2.1 a simplified soil-vegetation-atmosphere transfer scheme (SVATS) is developed by combining point representations of atmospheric forcing, vertical soil water transport, and plant control of transpiration. Model states include surface temperature, canopy water storage, moisture content in two soil layers, and the local water table depth as a lower boundary condition. In section 2.2 a spatially distributed, grid-based approach is employed to aggregate the simple SVATS to the catchment scale, which in this paper is defined as less than 100 km^2. An important assumption in moving from the point to the catchment scale is that explicit patterns of spatially variable model inputs and parameters can significantly affect catchment-scale hydrologic response. Another assumption is that spatial variability in topographic and soil properties dominates the process of downslope redistribution of soil water. Therefore the spatial pattern of the topographic-soil index [*Beven*, 1986] is employed to model the spatial pattern of water table depths [*Sivapalan et al.*, 1987], thus coupling the grid elements within the catchment through the process of saturated subsurface soil water flow. In section 2.3 a statistical-dynamical approach is utilized to simplify the large-scale modeling problem and to aggregate the SVATS to the macroscale, which is defined as the grid scale of an atmospheric model (10 km for mesoscale models to greater than 100 km for general circulation models, or GCMs). An implicit assumption at this scale is that a spatially distributed representation of important spatial variability (e.g., the topographic-soil index) can be replaced by a simpler, statistical representation. Such an assumption allows spatially variable runoff, and energy balance processes to be incorporated into the macroscale framework in a simple yet hydrologically realistic fashion.

The macroscale formulation is proposed for use as a land surface parameterization in atmospheric models. It differs greatly from vertically sophisticated Biosphere-Atmosphere Transfer Scheme (BATS) [*Dickinson et al.*, 1993] or Simple Biosphere Model (SiB) [*Sellers et al.*, 1986] type parameterizations by its simplified representation of vertical process physics and its statistical representation of horizontally heterogeneous runoff and energy balance processes. While an increasing number of land surface parameterizations are recognizing the importance of incorporating heterogeneity in hydrological processes (see *Avissar and Pielke* [1989], *Koster and Suarez* [1992], and A. S. Seth et al. (unpublished manuscript, 1993) for examples of "patch" representations of heterogeneity; and *Entekhabi and Eagleson* [1989] and

Famiglietti and Wood [1991b] for examples of statistical representations of heterogeneity) the macroscale formulation is one of very few new parameterizations [see also *Liang et al.*, 1994] to incorporate lateral subsurface soil water redistribution [*Pitman et al.*, 1993] and thus subgrid-scale spatial variability in the runoff and energy fluxes.

In section 3, the spatially distributed model formulation is explored to understand the role of spatial variability in determining areally averaged fluxes. The macroscale formulation is compared with the spatially distributed formulation to determine how it represents important spatial variability, with implications for parameterizing land surface water and energy balance processes in atmospheric models. Sections 4 and 5 contain a discussion and summary, respectively.

2. Model Descriptions

2.1. A Local Soil-Vegetation-Atmosphere Transfer Scheme

In this section a simple SVATS is briefly described. This local model is described in more detail by *Famiglietti* [1992]. The purpose of the model is to predict the diurnal dynamics of the water and energy fluxes at the land surface and to predict local vertical recharge to the water table. By necessity, the structure of the model is considerably more simple than currently operational SVATS, so that it can be applied repeatedly in space and time. For example, a spatially distributed model may require local water balance computations for hundreds of thousands of grid elements at small time increments. Therefore, the vertical soil moisture fluxes are represented using approximate analytical solutions to the governing equations for soil water flow in the unsaturated zone [*Richards*, 1931] in the manner of *Eagleson* [1978]. The resulting model structure is detailed enough, however, to represent the essential physics at the land-atmosphere interface.

The processes represented within the SVATS are shown in Figure 1. The land surface is partitioned into bare-soil and vegetated components. The vegetated component is assumed to be distributed uniformly over the surface. An interception store is maintained within the canopy so that wet and dry canopy are recognized. Evaporation and transpiration are computed for the wet and dry canopy, respectively. Evaporation is computed for the bare-soil component of the surface. The sensible and ground heat fluxes are also computed for the wet canopy, dry canopy, and bare soil but are not shown in Figure 1. Infiltration and surface runoff are computed for the bare soil and vegetated components of the land surface. Runoff generation in the model occurs by both the infiltration excess and saturation excess mechanisms.

The surface runoff and energy fluxes depend strongly on surface soil moisture. Consequently, the subsurface soil column is partitioned into two layers. An upper, more active root zone is modeled, which supplies the bare soil and vegetation with soil moisture for evapotranspiration. Its state of wetness also affects the magnitude of the infiltration and runoff fluxes. In addition to infiltration and evapotranspiration, two other root zone soil water fluxes are modeled. A drainage flux exits from the base of the root zone and enters the transmission zone. An upward flux of soil water from the water table due to capillary forces is modeled as well. Roots are assumed to extend uniformly throughout the root zone.

Beneath the root zone a lower, less active transmission zone is modeled. This zone extends from the base of the root zone to the top of the capillary fringe, which overlies the water table. The base of the transmission zone forms the lower boundary of the SVATS. Soil water fluxes through the transmission zone include the drainage flux from the root zone, which enters through the top of the transmission zone, and a drainage flux out of the transmission zone. The upward capillary flux from the water table passes through the transmission zone and into the root zone.

The model is driven with standard meteorological data at a time resolution high enough to resolve the diurnal dynamics of land-atmosphere interaction (1–2 hours). Driving data include precipitation, shortwave radiation, longwave radiation, pressure, humidity, air temperature, and wind speed. A summary and description of model parameters is found in Table 1. SVATS states include the depth of water stored in the canopy w_c; surface temperature T_s; moisture content in the root zone θ_{rz} (assumed uniform with depth); moisture content in the transmission zone θ_{tz} (also uniform with depth); and the local water table depth z (positive downward).

2.1.1. Local water balance equations.
Prognostic equations for the SVATS model states are given below.

Interception storage water balance equation: The water balance for the canopy is given by

$$dw_c/dt = p - e_{wc} - p_{net} \qquad 0 \le w_c \le w_{sc} \qquad (1)$$
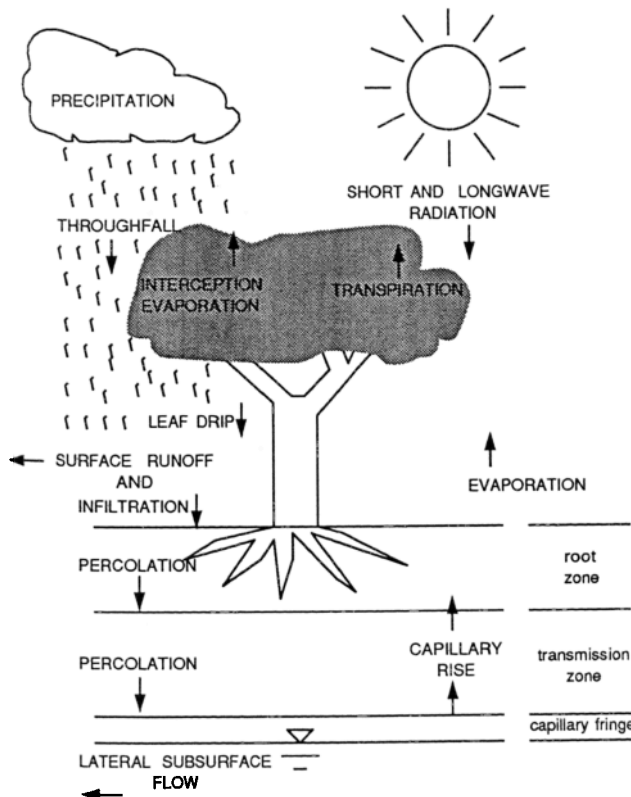
with

$$e_{wc} = \omega_{wc} e_{wct} \qquad (2)$$

Figure 1. Hydrological processes represented in the local SVATS.

Table 1. Model Parameters

Parameter	Description
	Soil
K_s, mm/s	saturated hydraulic conductivity
θ_s	saturation moisture content
θ_r	residual moisture content
B	pore size distribution index
ψ_c, m	air entry suction head
α	bare-soil albedo
D, m	damping depth of surface temperature wave
z_0, m	bare-soil roughness length
z_{rz}, m	root zone depth
	Vegetation
α	wet canopy albedo
α	dry canopy albedo
z_0, m	canopy roughness length
d, m	canopy zero plane displacement
r_{stmin}, s/m	minimum stomatal resistance
LAI	leaf area index
ψ_{crit}, m	critical leaf water potential
F	root activity factor
L, m/m	root density
R_u, s/m	root resistance
f_v	areal fraction of vegetation

where p is the precipitation rate, e_{wc} is the wet canopy evaporation rate, p_{net} is the net precipitation that occurs when the canopy water storage capacity w_{sc} has been exceeded, e_{wct} is the rate of evaporation from the entire wet canopy (described later), and ω_{wc} is the areal fraction of wet canopy, which is determined from *Deardorff* [1978] as

$$\omega_{wc} = (w_c/w_{sc})^{(2/3)} \qquad e_{wct} > 0 \qquad (3)$$

$$\omega_{wc} = 1 \qquad e_{wct} \le 0 \qquad (4)$$

The canopy water storage capacity is calculated after *Dickinson* [1984] as a function of the leaf area index LAI

$$w_{sc} = 0.0002 \text{ LAI} \qquad (5)$$

Soil description: Soil properties are modeled using the description proposed by *Brooks and Corey* [1964]. The five parameters utilized in this description include the saturated hydraulic conductivity K_S, the saturation moisture content θ_s, the residual moisture content θ_r, the pore size distribution index B, and the air entry suction head ψ_c. Soil moisture and hydraulic conductivity in unsaturated soils can be described in terms of the matric head ψ as

$$\theta(\psi) = \theta_r + (\theta_s - \theta_r)(\psi_c/\psi)^B \qquad \psi > \psi_c \qquad (6a)$$

$$K(\psi) = K_s(\psi_c/\psi)^{2+3B} \qquad \psi > \psi_c \qquad (6b)$$

$$K(\psi) = K_s \qquad \theta(\psi) = \theta_s \qquad \psi \le \psi_c \qquad (6c)$$

Soil water balance equations: To derive the soil water balance equations for the root and transmission zones, two specific cases with respect to local water table depth are considered. In case 1 the top of the capillary fringe lies beneath the bottom of the root zone at a depth $z - \psi_c$. The unsaturated zone is partitioned into a root zone of depth z_{rz} and an underlying transmission zone. The vertical distance between the top of the capillary fringe and the base of the root zone is defined as the transmission zone length z_{tz}. In case 2 the top of the capillary fringe lies within the root zone; there is no transmission zone in case 2.

The root zone water balance equation for case 1 is

$$z_{rz} \frac{d\theta_{rz}}{dt} = f_{bs}i_{bs} + f_v i_v + w - f_{bs}e_{bs} - f_v e_{dc} - g_{rz} \qquad (7a)$$

for

$$z - \psi_c \geq z_{rz} \qquad \theta_r \leq \theta_{rz} \leq \theta_s \qquad (7b)$$

where f_{bs} is the fraction of bare soil land surface, i_{bs} is the infiltration rate into bare soils, f_v is the fraction of vegetated land surface (equal to $1 - f_{bs}$), i_v is the infiltration rate into vegetated soils, w is the rate of capillary rise from the water table, e_{bs} is the evaporation rate from bare soils, e_{dc} is the dry canopy transpiration rate, g_{rz} is the downward soil water flux from the base of the root zone, and the remaining variables have been previously defined.

The water balance equation for the transmission zone is

$$z_{tz} \, d\theta_{tz}/dt = g_{rz} - g_{tz} \qquad z_{tz} > 0 \qquad (8a)$$

for

$$z_{tz} = z - \psi_c - z_{rz} \qquad \theta_r \leq \theta_{tz} \leq \theta_s \qquad (8b)$$

where g_{tz} is the downward soil water flux from the base of the transmission zone.

The root zone water balance equation for case 2 is

$$z_{rz}^* \frac{d\theta_{rz}}{dt} = f_{bs}i_{bs} + f_v i_v + w - f_{bs}e_{bs} - f_v e_{dc} - g_{rz} \qquad (9a)$$

for

$$z_{rz}^* = z - \psi_c \qquad z_{rz} > z - \psi_c \geq 0 \qquad \theta_r \leq \theta_{rz} \leq \theta_s \qquad (9b)$$

where θ_{rz} is the uniform moisture content which extends from the top of the capillary fringe to the land surface.

The actual infiltration rate for bare soil is taken as the minimum of an infiltration capacity $i^*(I)$, or the precipitation rate, such that

$$i_{bs} = \min [i^*(I), \, p] \qquad (10)$$

Actual infiltration into vegetated soil is the minimum of the infiltration capacity or the net rate of precipitation, so that

$$i_v = \min [i^*(I), \, p_{net}] \qquad (11)$$

The infiltration capacity for bare and vegetated soils is given by *Milly* [1986] in terms of cumulative infiltration I, soil properties, and the root zone moisture content at the start of each storm event.

The rate of capillary rise is based on the result of *Gardner* [1958] for steady upward flow from a water table

$$w = Ca/(z - \psi_c)^b \qquad (12)$$

where the parameters C, a, and b are functions of soil type and are given by *Eagleson* [1978] in terms of the *Brooks and Corey* [1964] soil parameters.

The actual rate of bare-soil evaporation is taken as the minimum of a soil-controlled exfiltration capacity $e^*(E_c)$, or the atmospherically controlled potential evaporation rate e_{pe} (defined later):

$$e_{bs} = \min [e^*(E_c), \, e_{pe}] \qquad (13)$$

The bare-soil exfiltration capacity is given by *Milly* [1986] as a function of cumulative exfiltration E_c, root zone moisture content at the start of an interstorm period, and soil properties.

The actual rate of transpiration from the dry canopy is obtained from the minimum of the vegetation-controlled transpiration capacity τ^*, or the atmospherically controlled unstressed transpiration rate t_{unst} (defined later), as

$$e_{dc} = \omega_{dc} \min [\tau^*, \, t_{unst}] \qquad (14)$$

where ω_{dc} is a canopy water balance variable which expresses the current areal fraction of dry canopy (equal to $1 - \omega_{wc}$). Thus the term vegetation control refers to a state of increased stomatal resistance beyond unstressed levels. The transpiration capacity is based on the soil water extraction model of *Feyen et al.* [1980], and is a function of the matric potential of the soil ψ_s; the critical leaf water potential ψ_{crit}; the hydraulic resistance of the soil R_S; and the hydraulic resistance of the plant R_p.

Drainage from the base of the root zone and transmission zone is assumed to proceed at gravity driven rates. These fluxes are described by

$$g_{rz} = K_S \left[\frac{\theta_{rz} - \theta_r}{\theta_s - \theta_r} \right]^\eta \qquad (15)$$

where

$$\eta = \frac{2 + 3B}{B} \qquad (16)$$

and g_{tz} is given by replacing θ_{rz} with θ_{tz} above.

Both saturation excess runoff and infiltration excess runoff are computed within the model. The bare soil and vegetated runoff fluxes are

$$q_{bs} = p \qquad \theta_{rz} = \theta_s \qquad (17a)$$

$$q_{bs} = p - i^*(I) \qquad \theta_{rz} < \theta_s \qquad p > i^*(I) \qquad (17b)$$

$$q_v = p_{net} \qquad \theta_{rz} = \theta_s \qquad (17c)$$

$$q_v = p_{net} - i^*(I) \qquad \theta_{rz} < \theta_s \qquad p_{net} > i^*(I) \qquad (17d)$$

Saturated zone water balance equations: The lower boundary condition of the SVATS is the top of the capillary fringe, which is controlled by the local water table depth. In this work, the space-time dynamics of the local water table depth are modeled using a spatially aggregated procedure. Therefore the water balance equation for the local water table depth is presented with the descriptions of the catchment-scale and macroscale models.

2.1.2. Local energy balance equations, potential evapotranspiration, and surface temperature. To determine the evapotranspiration rates e_{wc}, e_{dc}, and e_{bs}, the rate of evaporation from the entire wet canopy, the unstressed transpiration rate, and the potential evaporation rate for bare soils must first be computed. These potential rates of evapotranspiration are determined from energy balances for the wet canopy, dry canopy, and bare soils, respectively.

The horizontally homogeneous, one-dimensional form of the energy balance equation is

$$R_n = \rho_w LE + H + G \qquad (18)$$

where R_n is the net radiation, ρ_w is the density of liquid water, $\rho_w LE$ is the latent heat flux into the atmosphere, H is the sensible heat flux into the atmosphere, and G is the heat flux into the ground. Net radiation is given as

$$R_n = R_{sd}(1 - \alpha) + \varepsilon R_{ld} - \varepsilon \sigma T_l^4 \tag{19}$$

where R_{sd} is downward shortwave radiation, α is the albedo, ε is the emissivity, R_{ld} is the downward longwave radiation, σ is the Stefan-Boltzmann constant, and T_l is the temperature of the wet canopy, dry canopy, or bare-soil surface. Latent heat flux is given by *Milly* [1991] as

$$\rho_w LE = \frac{\rho c_p}{\gamma(r_c + r_{av})} (e^*(T_l) - e_a) \tag{20}$$

where ρ is the density of air, c_p is the specific heat of air at constant pressure, γ is the psychometric constant, r_c is the canopy resistance, r_{av} is the aerodynamic resistance, $e^*(T_l)$ is the saturation vapor pressure at the surface temperature T_l, and e_a is the vapor pressure at some level above the canopy or soil surface z_a. The flux of sensible heat is described by

$$H = (\rho c_p / r_{ah})(T_l - T_a) \tag{21}$$

where r_{ah} is the aerodynamic resistance to heat flow, and T_a is the air temperature at z_a. Ignoring the effects of heat storage in the surface soil layer, heat flux into the surface, G, is assumed to be a linear function of the subsurface temperature gradient and is given by

$$G = (\kappa/D)(T_l - T_2) \tag{22}$$

where κ is the thermal conductivity, D is the damping depth of diurnal temperature oscillations, and T_2 is temperature at depth D. The expression employed for thermal conductivity is dependent on matric head and is described by *McCumber and Pielke* [1981]. The temperature T_2 is presently prescribed in the model. The aerodynamic resistances are given by

$$r_{ah} = r_{av} = \frac{1}{k^2 u(z_a)} \left[\ln \left[\frac{(z_a - d)}{z_0} \right] \right]^2 \tag{23}$$

where k is von Kármán's constant, $u(z_a)$ is the wind speed at level z_a, d is the zero plane displacement, and z_0 is the roughness length of the canopy or the soil surface.

Evaporation from the entire wet canopy e_{wct} is determined by solving (18)–(23) for the temperature of the wet vegetated surface. Setting α, z_0, and d consistent with the type of wet vegetation, setting G and r_c equal to zero, and letting T_l represent the temperature of the wet vegetated surface yields the partitioning of R_n into $\rho_w LE$ and H. The unstressed transpiration t_{unst} is calculated in the same manner as e_{wct}, but with r_c representing canopy resistance as $r_c = r_{stmin}/\text{LAI}$, where r_{stmin} is a minimum value of stomatal resistance. The potential evaporation e_{pe} for bare soil is calculated using (18)–(23) with r_c equal to zero, α, z_0, and d consistent with the particular type of wet soil, and T_l applying to the temperature of the wet bare-soil surface.

The temperatures and fluxes thus determined are for potential or unstressed conditions. When stomatal resistance increases above its minimum level and the actual transpiration rate is less than the unstressed rate, e_{dc} is substituted

for E in (20), and (18) is resolved for the correct dry canopy temperature and fluxes. When bare-soil evaporation proceeds at soil-controlled rates, e_{bs} is substituted for E in (20), and (18) is resolved for the correct bare-soil temperature and energy fluxes.

2.1.3. Local water and energy balance fluxes. The local rates of evapotranspiration E and runoff Q are determined by summing the bare-soil and vegetated components, weighted by their corresponding areal fractions:

$$E = f_{bs} e_{bs} + f_v (e_{dc} + e_{wc}) \tag{24}$$

$$Q = f_{bs} q_{bs} + f_v q_v \tag{25}$$

The remaining energy fluxes and surface temperature are determined as in (24).

2.2. Aggregating the Local Model to the Catchment Scale

In this section, one approach to aggregating local process physics to the catchment scale is described. A key assumption in scaling up from the point to the catchment scale is that explicit patterns of spatially variable model inputs and parameters can significantly affect hydrologic response and must therefore be incorporated into models applied across these scales. Consequently, a spatially distributed model structure is developed for use at the catchment scale. While not theoretically limited to the catchment scale, the spatially distributed model structure may be operationally limited to this scale owing to computational constraints, the cumbersome nature of spatially distributed input and output data, and the lack of available large-scale, high-resolution data sets for model calibration and validation. Also, as was investigated by *Wood et al.* [1988] and in paper 3, explicit patterns of model inputs and parameters may not be required to adequately model the larger-scale water and energy balance. At these scales, a statistical representation of spatial variability in important model inputs and parameters may suffice.

The spatially distributed model formulation employs a digital elevation model to represent catchment topography. The catchment is discretized into grid elements based on the resolution of the digital elevation model (DEM) and the local SVATS is applied to each catchment grid. Spatially distributed fields of model parameters and inputs (e.g., atmospheric forcing, topographic, soil, and vegetation properties) are coregistered with the DEM so that spatial variability in model outputs (e.g., soil moisture, evapotranspiration, runoff) is represented explicitly (see Figure 2). The catchment-average hydrologic response is simply the average of the local grid element responses. This model is described in detail by *Famiglietti* [1992]. It extends the work of *Famiglietti et al.* [1992] by incorporating a more realistic and dynamic description of the water and energy balance between the water table and the top of the canopy (the SVATS of the preceding section) while maintaining a simple, computationally efficient model structure.

Since the SVATS requires the local water table depth as a lower boundary condition, the spatially distributed model framework requires the spatial pattern of water table depths to couple grid elements together at the catchment scale. A simplified, topographically based methodology for computing and updating the catchment-scale pattern of water table depths is employed. The topographic-soil index of *Beven*
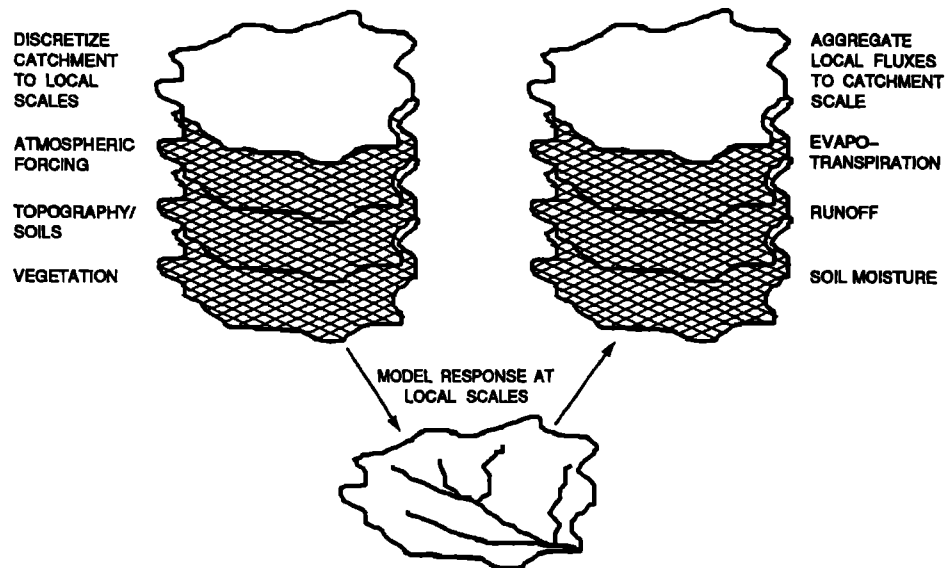
Figure 2. Schematic representation of catchment disaggregation and aggregation in the spatially distributed modeling approach.

[1986] is utilized to parameterize spatial variability in topographic and soil properties, and thus water table depth, between catchment grid elements. This procedure is reviewed in section 2.2.1.

The model uses the same parameters as the local SVATS (see Table 1) and is driven with the same standard meteorological data. However, the model structure can now accommodate spatially distributed fields of parameter and forcing data when available. The model computes N interception storages, surface temperatures, root and transmission zone moisture contents, and local water table depths to determine N values of surface runoff and the latent, sensible, and ground heat fluxes, where N is the number of catchment grid elements. In the remainder of this section we describe in more detail how catchment grid elements are coupled together and how the catchment-scale water and energy balances are computed.

2.2.1. Lateral subsurface flow and water table dynamics. All soil water transport in the unsaturated zone is assumed vertical and noninteractive between grid elements. However, as was mentioned above, a simple topographic framework is employed to compute saturated subsurface flow between grid elements and the spatial pattern of local water table depths. These dynamics are important for a number of reasons. Each grid element in the catchment requires the local water table depth as the lower boundary condition for the local SVATS. The local water table depth will affect local soil moisture storage and thus the root zone moisture content and the surface hydrologic fluxes. When the water table reaches the land surface along stream channel grid elements, the land surface becomes saturated. Evaporation and transpiration from saturated areas proceed at potential rates. All rainfall on these areas is transformed into saturation excess runoff. Therefore modeling water table dynamics is an important link in accurately predicting the catchment-scale water and energy balance.

We assume that saturated subsurface flow between catchment grid elements is controlled by the spatial variability in topographic and soil properties and employ the topographic-

soil index to parameterize this variation. The topographic-soil index is a local drainage index derived for quasi-steady state conditions. *Sivapalan et al.* [1987] derived a simple expression for the local water table depth z^i in terms of the local topographic-soil index, $\ln \{(aT_e)/(T^i \tan \beta)\}$:

$$z^i = \bar{z} - \frac{1}{f}\left\{ \ln\left(\frac{aT_e}{T^i \tan \beta}\right) - \lambda \right\} \qquad (26)$$

where $\bar{z}$ is the catchment average water table depth, i is the local grid element index, f is a parameter that describes the exponential decay of saturated hydraulic conductivity with depth, a is the area drained through the local unit contour, T_e is the catchment average value of the saturated transmissivity coefficient (saturated hydraulic conductivity divided by f), T^i is the local value of the transmissivity coefficient, β is the local slope angle, and λ is the catchment average value of the topographic variable $\ln (a/\tan \beta)$. The spatial distribution of the topographic-soil index can be computed for a region using a DEM and regional soil survey information. A number of algorithms have been developed by government and university research groups to extract such geomorphologic information. Commercial geographic information system packages can also be utilized for this purpose.

For any particular value of $\bar{z}$, (26) shows that high values of the topographic-soil index imply a tendency toward surface saturation ($z^i \leq \psi_c^i$). High values of the index are generally associated with zones of topographic convergence, areas with large a, low β, or low saturated hydraulic conductivity. Conversely, low values of the index imply a deeper water table. Therefore knowledge of the spatial distribution of the topographic-soil index allows prediction of the spatial distribution of water table depths. Modeling the temporal changes in $\bar{z}$ allows the spatial distribution, including the areal extent of hydrologically active saturated areas, to be updated in time. This updating procedure is analogous to a simplified model of lateral subsurface soil water flow in the saturated zone.

2.2.2. Local water and energy balance equations.

Local SVATS equations (1)–(25) are applied to each grid element in the catchment to compute local water and energy balances. To properly apply the soil water balance equations, three specific regions within the catchment are recognized. Region 1 consists of grid elements where the top of the capillary fringe lies beneath the bottom of the root zone. SVATS case 1 soil water balance equations are applied in region 1. In region 2 the top of the capillary fringe lies within the root zone; there is no transmission zone in region 2. The appropriate soil water balance equations for region 2 are SVATS case 2 equations. Region 3 consists saturated grid elements where $z^i \le \psi_c^i$. In this region the root zone remains saturated, so that

$$z_{rz} \, d\theta_{rz}^i/dt = 0 \qquad z^i - \psi_c^i < 0 \qquad (27)$$

$$\theta_{rz}^i = \theta_s^i$$

and as in region 2, there is no transmission zone.

2.2.3. Saturated zone water balance equation.

Equation (26) shows that the rate of change of the local water table depth dz^i/dt is equal to $d\bar{z}/dt$, the rate of change of the areal average water table depth. This quantity was derived by global mass balance considerations for the discretized catchment as $\Delta z/\Delta t$, which we use to approximate the differential $d\bar{z}/dt$ as

$$\frac{d\bar{z}}{dt} \approx \frac{\Delta z}{\Delta t}$$

$$= \left[\sum_{i \in \mathfrak{R}_1, \mathfrak{R}_2} w^i + \sum_{i \in \mathfrak{R}_3} E^i + Q_b/(\Delta x \Delta y) - \sum_{i \in \mathfrak{R}_1} g_{tz}^i - \sum_{i \in \mathfrak{R}_2} g_{rz}^i \right]$$

$$\cdot \left[\sum_{i \in \mathfrak{R}_1} (\theta_s^i - \theta_{tz}^i) + \sum_{i \in \mathfrak{R}_2} (\theta_s^i - \theta_{rz}^i) \right]^{-1} \qquad (28)$$

where regions 1, 2, and 3 are represented by $\mathfrak{R}_1$, $\mathfrak{R}_2$, and $\mathfrak{R}_3$; Q_b is base flow; and $\Delta x \Delta y$ is the area of a grid element.

Depletions of saturated zone storage result from the sum of the capillary flux from regions 1 and 2, $\sum_{i \in \mathfrak{R}_1, \mathfrak{R}_2} w^i$; evapotranspiration from region 3, $\sum_{i \in \mathfrak{R}_3} E^i$; and base flow Q_b, which is defined in the next section. Recharge to the water table results from the sum of the transmission zone drainage flux over region 1, $\sum_{i \in \mathfrak{R}_1} g_{tz}^i$, and the sum of the root zone drainage flux over region 2, $\sum_{i \in \mathfrak{R}_2} g_{rz}^i$. The terms in the denominator of (28) represent the catchment storage deficit in the transmission and root zones, respectively.

2.2.4. Catchment-scale water and energy balance fluxes.

The catchment-scale water and energy balance fluxes are simply the average of the grid element fluxes. The catchment-scale evapotranspiration rate $\bar{E}$ is

$$\bar{E} = \frac{1}{N} \sum_{i \in \mathfrak{C}} E^i = \frac{1}{N} \sum_{i \in \mathfrak{C}} [f_{bs}^i e_{bs}^i + f_v^i (e_{dc}^i + e_{wc}^i)] \qquad (29)$$

where $\mathfrak{C}$ is the set of all grid elements in the catchment. The remaining catchment-scale energy fluxes are determined by similar averaging. The catchment-scale runoff rate $\bar{Q}$ is the average of local bare-soil and vegetated runoff components. A lateral subsurface flow component Q_b is also included in the catchment-scale flux. The catchment-scale runoff rate is

$$\bar{Q} = \frac{1}{N} \sum_{i \in \mathfrak{C}} Q^i + \frac{Q_b}{A} = \frac{1}{N} \sum_{i \in \mathfrak{C}} [f_{bs}^i q_{bs}^i + f_v^i q_v^i] + \frac{Q_b}{A} \qquad (30)$$

where A is the catchment surface area. Base flow is determined for the catchment by integrating the local saturated subsurface fluxes along the channel network, yielding [Sivapalan et al., 1987]

$$Q_b = Q_0 \exp (-f\bar{z}) \qquad (31)$$

where

$$Q_0 = AT_e \exp (-\lambda)$$

The parameters Q_0 and f, as well as the spatial distribution of the topographic-soil index, are required to operate the model in addition to those parameters listed in Table 1. Techniques for estimating Q_0 and f are described by Famiglietti et al. [1992].

Catchment-scale water balance is maintained by ensuring that water storage changes in the canopy, unsaturated zone, and saturated zone are equal to the sum of precipitation less evapotranspiration and runoff. Catchment-scale energy balance is guaranteed by enforcing $R_n^i - G^i - \rho_w LE^i - H^i = 0$ at each catchment grid element.

2.3. Aggregating to the Macroscale

Explicit aggregation using a high-resolution spatially distributed hydrological model is simply not feasible for use at the grid scale of regional and global atmospheric models. However, subgrid-scale spatial variability in certain land surface properties and processes will have a significant impact on the grid-scale water and energy fluxes and must somehow be represented within macroscale models. The question of which heterogeneities dominate land-surface response at the macroscale, and how to incorporate these heterogeneities into land-surface parameterizations, is a central issue in the development of these models. Spatial variability in vegetation, topography, rainfall, soil moisture, etc., acts in concert to produce the grid-scale fluxes. The relative roles of these variables likely change with geographic location and space-time scale. The work presented in this paper is directed in part at developing modeling tools to address these questions.

In this section a second approach to the aggregation problem is described which is appropriate for use at the macroscale. At such large scales the modeling problem must be simplified to maintain computational efficiency and so that the resulting parameterization can be incorporated into atmospheric models, which already have tremendous computational overhead. The approach described here is to identify important land surface heterogeneity, and to simplify its representation within a macroscale model (e.g., statistical rather than spatially distributed). Because we are interested in improving both runoff and energy balance in grid-scale models, we propose that subgrid-scale spatial variability in root zone soil moisture content is a dominant control on the grid-scale water and energy balance. The spatial distribution of root zone soil moisture determines the location, type, and magnitude of the surface runoff fluxes; it also determines which land surface regions evaporate at potential rates versus lower magnitude soil- and vegetation-controlled rates. To model these soil moisture dynamics, we

assume that subgrid-scale variations in topography and soils dominate the process of spatial redistribution of soil water over large land areas. A second assumption at the macro-scale is that a threshold modeling scale has been exceeded, so that the exact pattern of topographic and soil heterogeneities need not be represented explicitly within the model structure; at this scale a statistical representation of the variability will suffice. The existence of this threshold scale, called a representative elementary area (REA) [Wood et al., 1988], and the validity of the assumptions outlined above, have been investigated for runoff and evapotranspiration modeling by Wood et al. [1988] and in paper 3, respectively.

Based on these assumptions, a statistical distribution of the topographic-soil index is employed as the framework of this parameterization because it is representative of subgrid-scale spatial variability in topographic and soil properties. The distribution of the index is discretized into a number of intervals and the local SVATS is applied at each interval. Equation (26) provides the local water table depth for each interval of the distribution, effectively coupling intervals together through the process of saturated lateral subsurface flow. The macroscale hydrologic fluxes are the weighted average of the local fluxes, where the local weighting function is the probability of occurrence of the particular interval, i.e., grid-scale fluxes are determined by aggregating local fluxes with respect to the statistical distribution of the topographic-soil index (statistical aggregation). Note that the topographic index methodology is based on the concept of hydrologic similarity [Sivapalan et al., 1987; Wood et al., 1990], which suggests that locations with the same value of the topographic-soil index exhibit a similar hydrologic response. This set of papers represents a first step toward applying the concepts of similarity and an REA, which were developed in the context of storm response modeling, to interstorm evapotranspiration and energy balance modeling. Taken together, these concepts allow spatially variable runoff and energy balance processes to be incorporated into the macroscale framework in a simple yet hydrologically realistic fashion.

The model presented here, while not as vertically sophisticated as BATS/SiB type parameterizations, is still detailed enough to represent the essential physics of land-atmosphere interaction at a point. It also differs from these, essentially "point" models of land hydrological processes by its statistical representation of many land surface points and thus lateral heterogeneity in runoff and energy balance processes. The model builds upon the work of Famiglietti and Wood [1991b] by coupling a more realistic description of the local soil–vegetation–atmosphere water-energy balance to a TOP-MODEL framework [Sivapalan et al., 1987; Beven, 1986; Beven and Kirkby, 1979], thereby extending a successful runoff parameterization for simulation of large-scale land surface-atmosphere interaction. The resulting macroscale model, called TOPLATS (TOPMODEL-Based Land Atmosphere Transfer Scheme), incorporates subgrid-scale spatial variability in topography and soils to model downslope redistribution of soil water. In addition to providing a realistic representation of runoff processes, the redistribution of subsurface soil water feeds back through the model structure to yield subgrid variability in water table depth, soil water storage, root zone soil moisture content, and surface energy fluxes. This model is presented in detail by Famiglietti [1992] and is briefly reviewed below. This de-scription is followed by a presentation of the macroscale saturated zone water balance equation and the macroscale flux equations.

2.3.1. Conceptual overview of macroscale model framework.
The model framework requires a statistical representation of subgrid-scale spatial variability in the topographic-soil index. The distribution can be characterized in two ways: by its probability density function (pdf) or by its actual sample histogram. Sivapalan et al. [1987] showed that spatial variability in the topographic-soil index can be represented with a three-parameter gamma (μ, ϕ, χ), where μ, ϕ, and χ are the location, shape, and scale parameters of the distribution, respectively. They also showed that these parameters can be obtained from a DEM and an estimate of the variance of the saturated hydraulic conductivity. A pdf representation of the distribution facilitates the development of analytical water and energy balance equations. Alternatively, an actual sample histogram can be constructed from the DEM and digital soil survey information.

To perform water and energy balance computations, the distribution of the topographic-soil index is discretized into a number of intervals. Each interval of the distribution represents the fraction of land-surface area having a particular water table depth and subsurface soil moisture storage. The local SVATS is applied to each interval of the distribution. This procedure is shown schematically in Figure 3. The spatial distribution of the topographic-soil index is shown in Figure 3a for the 15-km FIFE site at 30-m resolution. Dark regions in this image correspond to high values of the index, such as those located along stream networks where the water table is high. Light regions correspond to low values of the index, such as those located near ridge tops, where the water table is deeper. The spatial distribution is characterized by the discretized pdf shown in Figure 3b, where $f(x)$ is the probability density function of $x = \ln\{(aT_e)/(T_x \tan \beta)\}$, and x refers to the representative value of the topographic-soil index for the interval. In Figure 3c, corresponding modeled soil-vegetation columns are shown for intervals with $x = 7$ (drier, with a lower water table and greater available soil water storage) and $x = 13$ (wetter, with a higher water table and less available soil water storage). SVATS equations applied at each interval of the distribution yield a local water and energy balance with a distinct surface temperature $T_s(x)$, root zone moisture content $\theta_{rz}(x)$, transmission zone moisture content $\theta_{tz}(x)$, water table depth $z(x)$, and runoff and energy flux rates ($Q(x)$, $LE(x)$, $H(x)$, and $G(x)$).

To draw a rough analogy to land-surface hydrologic "bucket" models, this model treats the grid-scale hydrologic behavior of the land surface as a distribution of interacting buckets, whose states of wetness vary with topography, soil properties, and water table depth. Buckets are interacting because as the areal average water table depth varies in time, by (26), so do the local water table depths and soil water storages. This process is analogous to downslope redistribution of soil water in the saturated zone. The distribution of buckets concept is evident in Figure 3. In moving from ridge crests to valley bottoms, or from low values of the index to high, the local water table depth decreases, the local unsaturated water storage decreases, and the local root zone moisture content increases. The local hydrologic fluxes which depend on root zone moisture content will therefore vary between intervals of the distribution. The resulting
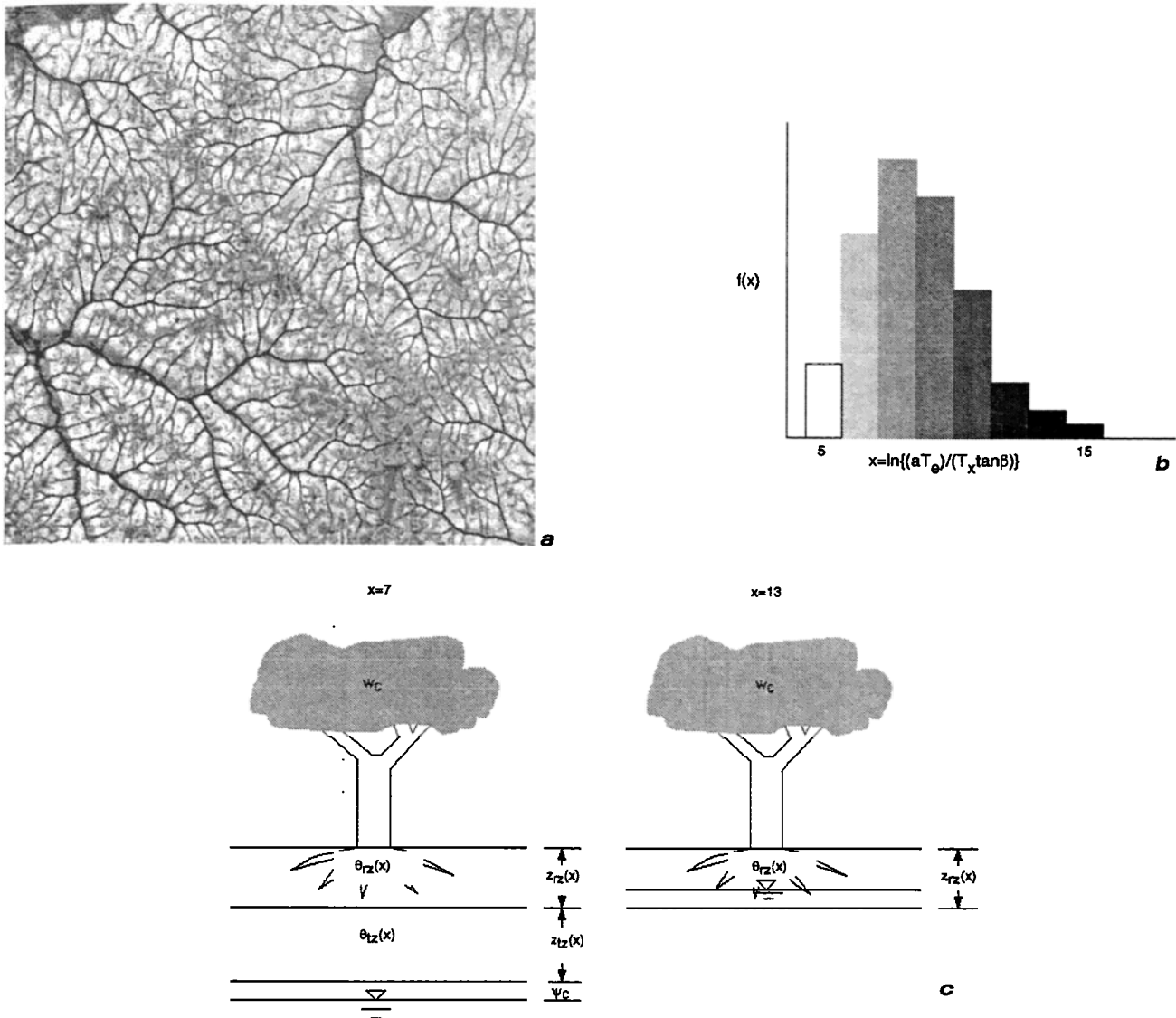
Figure 3. Conceptual framework of macroscale model. (a) Spatial distribution of the topographic-soil index for the 15-km FIFE site, 30-m resolution, north is at top of page. (b) Discretized pdf which characterizes the spatial distribution at left; $f(x)$ is the probability density function of $x = \ln \{(aT_e)/(T_x \tan \beta)\}$, and x is the value of the topographic-soil index for the interval. (c) Corresponding modeled soil-vegetation columns for $x = 7$ and $x = 13$.

large-scale hydrologic response is simply a weighted average of the responses of the individual buckets, or intervals of the distribution.

The macroscale model is driven with the same standard meteorological data and uses the same parameters as the local SVATS (see Table 1). Areal average values of these data are used because of the desire to maintain a simplified model structure. Therefore only one set of model forcing computations are required per time step, rather than one set for each interval of the distribution. The bias induced by this approach can be determined by comparing detailed model simulations using the spatially distributed model with those produced by the simpler macroscale model. *Famiglietti and Wood* [this issue] and paper 3 provide an example of such comparisons for small a watershed at the FIFE site. A methodology to reduce potential biases at larger scales is proposed in the discussion section. Additional model param-

eters include some description of the statistical distribution of the topographic-soil index, either using a pdf or histogram, and Q_0 and f, the base flow parameters.

2.3.2. Saturated zone water balance equation. As with the catchment-scale model, updating the spatial distribution of water table depths requires updating the areal average water table depth. The macroscale updating procedure is analogous to the catchment-scale procedure and involves balancing recharge and depletions to the saturated soil reservoir. Equation (28) is recast here in statistical, macroscale form.

First, some notation regarding the maximum values of $\ln \{(aT_e)/(T_x \tan \beta)\}$ in regions 1 and 2 is defined. The variable x^{sat} refers to the value of the topographic-soils index at which the land surface is just saturated, i.e., the maximum value of $\ln \{(aT_e)/(T_x \tan \beta)\}$ in region 2. From (26) this is given by

$$x^{\text{sat}} = \lambda - f(\psi_c - \bar{z}) \qquad (32)$$

Locations where $\ln\{(aT_e)/(T_x \tan \beta)\}$ is greater than x^{sat} are saturated. The variable x^{rz} refers to the maximum value of $\ln\{(aT_e)/(T_x \tan \beta)\}$ in region 1. When $\ln (aT_e/T_x \tan \beta)$ is greater than x^{rz} the top of the capillary fringe either lies within the root zone or at the soil surface. From (26), x^{rz} is given as

$$x^{rz} = \lambda - f(\psi_c + z_{rz} - \bar{z}) \qquad (33)$$

The rate of change of the areal average water table depth is

$$
d\bar{z}/dt = \left[\int_{x=-\infty}^{x=x^{\text{sat}}} w(x) f_x(x)\ dx + \int_{x=x^{\text{sat}}}^{x=\infty} E(x) f_x(x)\ dx \right.
$$

$$
+ Q_b/A - \int_{x=-\infty}^{x=x^{rz}} g_{tz}(x) f_x(x)\ dx
$$

$$
\left. - \int_{x=x^{rz}}^{x=x^{\text{sat}}} g_{rz}(x) f_x(x)\ dx \right]
$$

$$
\div \left[\int_{x=-\infty}^{x=x^{rz}} (\theta_s - \theta_{tz}(x)) f_x(x)\ dx \right.
$$

$$
\left. + \int_{x=x^{rz}}^{x=x^{\text{sat}}} (\theta_s - \theta_{rz}^*(x)) f_x(x)\ dx \right] \qquad (34)
$$

Saturated zone storage is depleted by the aggregated flux of capillary rise from regions 1 and 2, $\int_{x=-\infty}^{x=x^{\text{sat}}} w(x) f_x(x)\ dx$, evapotranspiration from saturated regions, $\int_{x=x^{\text{sat}}}^{x=\infty} E(x) f_x(x)\ dx$, and base flow, Q_b. The water table is recharged by the downward flux from the transmission zone aggregated over region 1, $\int_{x=-\infty}^{x=x^{rz}} g_{tz}(x) f_x(x)\ dx$, and the downward flux from the root zone aggregated over region 2, $\int_{x=x^{rz}}^{x=x^{\text{sat}}} g_{rz}(x) f_x(x)\ dx$. The terms in the denominator represent the areal average storage deficit from the transmission and root zones, respectively.

2.3.3. Macroscale water and energy balance fluxes. The grid-scale water and energy balance fluxes are determined by the aggregation procedure described previously: land-surface fluxes for each interval of the distribution are computed and weighted by the probability of occurrence of the interval. Using this procedure, the expected macroscale evapotranspiration rate $E[E]$ can be expressed analytically as

$$E[E] = \int_{x=-\infty}^{x=\infty} E(x) f_x(x)\ dx$$

$$= \int_{x=-\infty}^{x=\infty} [f_{bs} e_{bs}(x) + f_v(e_{dc}(x) + e_{wc})] f_x(x)\ dx \qquad (35)$$

where $E(x)$ is the local evapotranspiration rate for a particular interval of the distribution. The expected value of them surface temperature and the remaining energy balance fluxes are expressed in similar fashion. The expected macroscale runoff rate $E[Q]$ is expressed as

$$E[Q] = \int_{x=-\infty}^{x=\infty} Q(x) f_x(x)\ dx + Q_b$$

$$= \int_{x=-\infty}^{x=\infty} [f_{bs} q_{bs}(x) + f_v q_v(x)] f_x(x)\ dx + Q_b \qquad (36)$$

where $Q(x)$ is the local surface runoff rate for a particular interval of the distribution.

3. Effect of Spatial Variability on Catchment-Scale and Macroscale Fluxes

In this section we explore the role of spatial variability in determining modeled catchment-scale and macroscale runoff and evapotranspiration fluxes. Catchment-scale flux equations (29) and (30) and macroscale flux equations (35) and (36) are expanded to better understand how natural land surface heterogeneity affects the dynamics of land surface-atmosphere interaction, and how this is represented within the model structures. A key assumption in this section is that the spatially distributed model formulation presents a detailed picture of the dynamics of hydrological processes, so that the effect of our simplifying assumptions at the macroscale can be determined by comparison. In this section we focus on comparison of model formulations. *Famiglietti and Wood* [this issue] and paper 3 compare simulations with both models using observed data.

3.1. Spatial Variability and the Catchment-Scale Fluxes

3.1.1. Catchment-scale evapotranspiration rates. The catchment-scale evapotranspiration rate $\bar{E}$ can be rewritten as

$$\bar{E} = \bar{E}_{wc} + \bar{E}_{dc} + \bar{E}_{bs} \qquad (37)$$

where $\bar{E}_{wc}$ is the catchment-scale wet canopy evaporation rate, $\bar{E}_{dc}$ is the catchment-scale transpiration rate, $\bar{E}_{bs}$ is the catchment-scale bare-soil evaporation rate,

$$\bar{E}_{wc} = \frac{1}{N} \left[\sum_{i \in \mathfrak{C}} f_v^i e_{wc}^i \right] \qquad (38)$$

$$\bar{E}_{dc} = \frac{1}{N} \left[\sum_{i \in \mathfrak{R}_3} f_v^i \omega_{dc}^i t_{\text{unst}}^i + \sum_{i \in \mathfrak{R}_1, \mathfrak{R}_2 | \tau^{*i} \geq t_{\text{unst}}^i} f_v^i \omega_{dc}^i t_{\text{unst}}^i \right.$$

$$\left. + \sum_{i \in \mathfrak{R}_1, \mathfrak{R}_2 | \tau^{*i} < t_{\text{unst}}^i} f_v^i \omega_{dc}^i \tau^{*i} \right] \qquad (39)$$

$$\bar{E}_{bs} = \frac{1}{N} \left[\sum_{i \in \mathfrak{R}_3} f_{bs}^i e_{pe}^i + \sum_{i \in \mathfrak{R}_1, \mathfrak{R}_2 | e^*(E_c)^i \geq e_{pe}^i} f_{bs}^i e_{pe}^i \right.$$

$$\left. + \sum_{i \in \mathfrak{R}_1, \mathfrak{R}_2 | e^*(E_c)^i < e_{pe}^i} f_{bs}^i e^*(E_c)^i \right] \qquad (40)$$

Equations (38)–(40) show that spatial variability in model inputs, parameters, and states results in three broad classifications of evapotranspiration from the land surface. The first summation terms in (39) and (40) represent evapotranspiration from saturated grid elements. Saturated locations have no trouble meeting the atmospheric demand for water

vapor and yield evapotranspiration at potential rates. Within saturated regions, evapotranspiration rates vary spatially with the potential rates, vegetated and bare soil fractions, and amount of wet versus dry canopy. The second summation terms in (39) and (40) show that outside the region of saturated land surface, an additional areal fraction of land surface produces evapotranspiration at potential rates. In these unsaturated grid elements, evapotranspiration proceeds at potential rates when local transpiration capacities or local exfiltration capacities exceed their potential rates. The areal extent of this region depends on the spatial distribution of potential evapotranspiration rates and the spatial distributions of exfiltration and transpiration capacities, which themselves depend on spatial variability in root zone soil moisture, soil, and vegetation properties. The areal extent of this region may also vary with the diurnal cycle of potential evapotranspiration, as is shown below. The third terms in (39) and (40) represent evapotranspiration by relatively dry unsaturated grid elements where local exfiltration and transpiration capacities are less than local potential evapotranspiration rates. Evapotranspiration within this region proceeds at soil- or vegetation-controlled rates. The areal extent of this region complements that of the region described above so that it shares the same controls. Within this region, rates of soil- or vegetation-controlled evapotranspiration vary spatially with root zone soil moisture, soil and vegetation properties, vegetated and bare-soil fractions, and the amount of wet versus dry canopy.

Figure 4 shows simulated diurnal dynamics of atmosphere versus soil-controlled evaporation for the King's Creek catchment on October 7, 1987. The King's Creek catchment is an 11.7 km^2 grassland watershed located near Manhattan, Kansas, in the northwest quadrant of the FIFE site. The experiment is fully described by *Sellers et al.* [1992]. Since our purpose here is simply to demonstrate how the model captures important process dynamics, the details of the simulation are not presented here but are discussed by *Famiglietti and Wood* [this issue]. Figures 4a to 4e represent time steps in the early morning (1215 UT), midmorning, noon, midafternoon, and early evening (0015 UT). These images were extracted from a 12-day simulation of water and energy balance run at half-hourly time steps from October 5 to 16, 1987. The dark grey color represents grid elements that evaporate at atmosphere-controlled potential rates. In (39) these locations correspond to the second summation term, since there were no saturated regions within the catchment at that time. The lighter grey color represents catchment locations that evaporate at lower, soil-controlled rates. These grid elements correspond to the third summation term in (39). This sequence of images shows how spatial variability in the land surface and the atmosphere interact to yield the actual evaporation from the catchment. In the morning, when the potential evaporation rates are low, most of the catchment evaporates at these potential rates. As potential evaporation rates increase in the late morning, the exfiltration capacities at drier grid elements are exceeded. These locations switch to soil-controlled evaporation. By midday, only the wettest grid locations can evaporate at potential rate. In this simulation, these locations are found along the stream network. As potential evaporation rates decrease in the late afternoon and evening, more grid locations within the catchment return to atmosphere-controlled

evaporation. Simulations of transpiration by vegetation display analogous dynamics, but are not shown here.

The fact that downslope redistribution of soil water is an important control on runoff generation is well understood. However, Figure 4 presents a strong visual case that lateral redistribution of soil water is an important control on the spatial distribution of evapotranspiration rates as well. Furthermore, the nonlinearities associated with the exfiltration–transpiration capacity–soil moisture relationships suggest that when soil and vegetation controls of evapotranspiration are active (e.g., during midday hours in Figure 4) catchment-scale evapotranspiration cannot be modeled using an areally averaged value of root zone moisture content. Rather, some recognition of the spatial distribution of root zone moisture content, including wetter areas located downslope, may be required to realistically model catchment-scale evapotranspiration. This point is investigated at the King's Creek catchment in paper 3. The relative roles of spatially variable vegetation, soils, and solar radiation are explored as well.

3.1.2. Catchment-scale runoff rates.

The spatially distributed model formulation yields the following expression for $\bar{Q}$, the catchment-scale runoff rate:

$$\bar{Q} = \bar{Q}_{bs} + \bar{Q}_v + \bar{Q}_b \qquad (41)$$

where $\bar{Q}_{bs}$ is the catchment-scale bare-soil runoff rate, $\bar{Q}_v$ is the catchment-scale runoff rate for vegetated soils,

$$\bar{Q}_{bs} = \frac{1}{N}\left[\sum_{i\in\mathfrak{R}_3} f^i_{bs}p^i + \sum_{i\in\mathfrak{R}_1,\mathfrak{R}_2|p^i>i^*(I)^i} f^i_{bs}(p^i - i^*(I)^i)\right] \qquad (42)$$

$$\bar{Q}_v = \frac{1}{N}\left[\sum_{i\in\mathfrak{R}_3} f^i_v p^i_{net} + \sum_{i\in\mathfrak{R}_1,\mathfrak{R}_2|p^i_{net}>i^*(I)^i} f^i_v(p^i_{net} - i^*(I)^i)\right] \qquad (43)$$

and $\bar{Q}_b = Q_b/A$. Equations (42) and (43) show that spatial variability at the land surface leads to spatial variability in the type and magnitude of runoff generated within the catchment. The first summation term on the right-hand side of both (42) and (43) represents saturation excess runoff, which occurs when rain falls on saturated grid elements. Within the saturated region, the magnitude of this flux varies spatially with precipitation intensity and bare and vegetated soil fractions. The second summation term on the right-hand side of both (42) and (43) represents infiltration excess runoff, which occurs when local precipitation rates exceed local infiltration capacities in unsaturated catchment locations. Within the unsaturated region, the magnitude of this flux varies spatially with precipitation rates, bare and vegetated soil fractions, and infiltration capacities. The areal extent of the regions which generate infiltration excess or saturation excess runoff varies in time with the spatial distributions of both surface soil moisture and precipitation intensity.

To demonstrate the model representation of these dynamics, a 2-day storm event (August 12–13, 1987) was simulated for the King's Creek catchment using half-hourly time steps. Details of the simulation, model inputs and parameters are described by *Famiglietti and Wood* [this issue]. Figure 5 shows the locations and rates of runoff generation for the two time steps of peak precipitation intensity (0145 UT (Figure 5 (left)) and 0215 UT (Figure 5 (right)). Catchment-
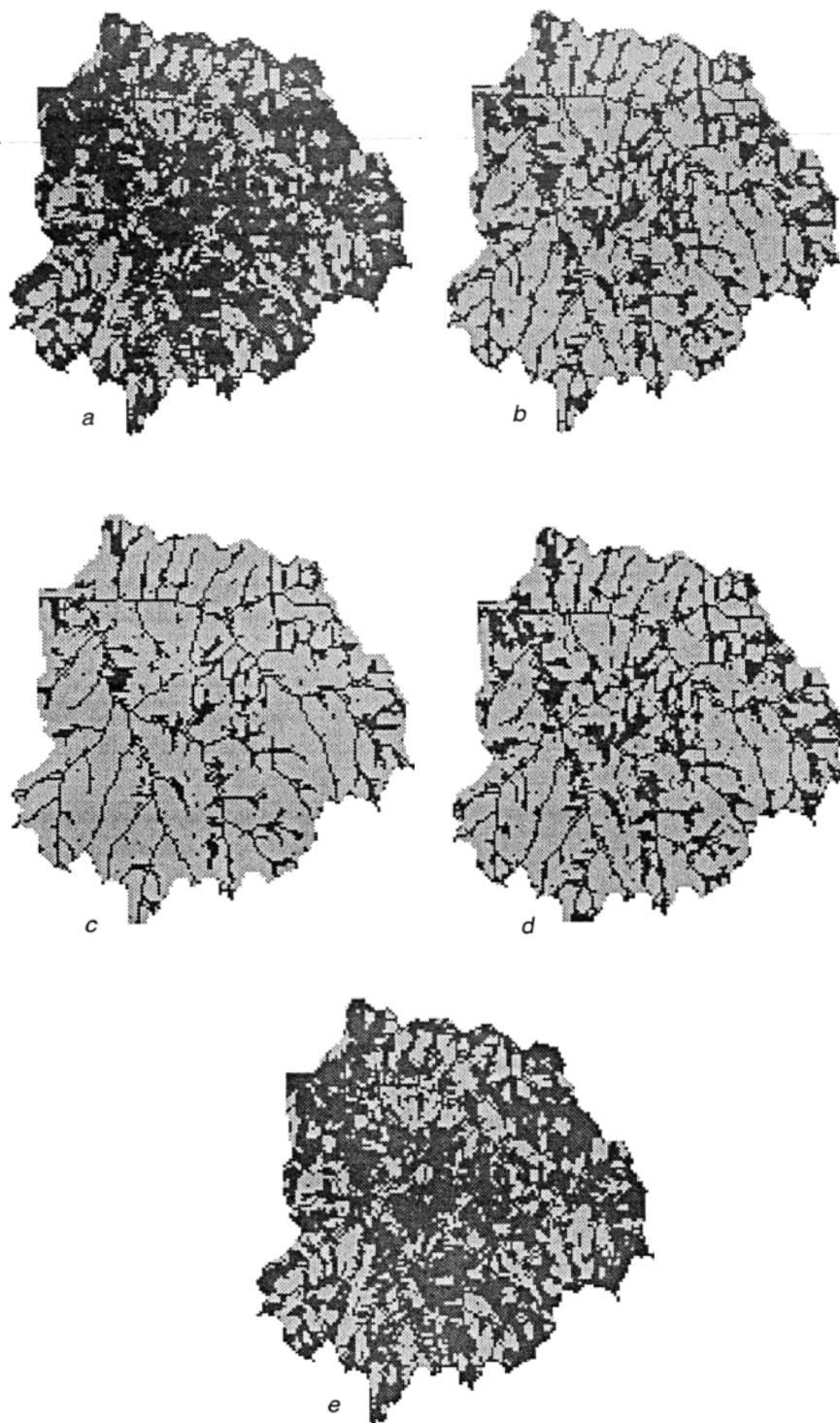
Figure 4. Diurnal dynamics of modeled bare-soil evaporation for the King's Creek catchment on October 7, 1987. Dark grey represents grid elements that evaporate at atmosphere-controlled potential rates. Light grey represents catchment locations that evaporate at lower soil-controlled rates. (a) Early morning (1215 UT), (b) midmorning, (c) noon, (d) midafternoon, and (e) early evening (0015 UT). Catchment area is 11.7 km^2, grid-element resolution is 30 m; north is at top of page.

average rainfall rates for these times were 51 mm/h and 40 mm/h, respectively. The scale black to white represents runoff generation rates from 30 mm/h to near 0 mm/h. The medium grey background represents the remaining catchment grid elements where no surface runoff was generated.

In the simulation, all runoff is produced by the infiltration excess mechanism: at this point in the summer there were no saturated regions within the catchment. The increase in the number of surface runoff producing locations between Figures 5a and 5b corresponds to the decrease in local infiltra-
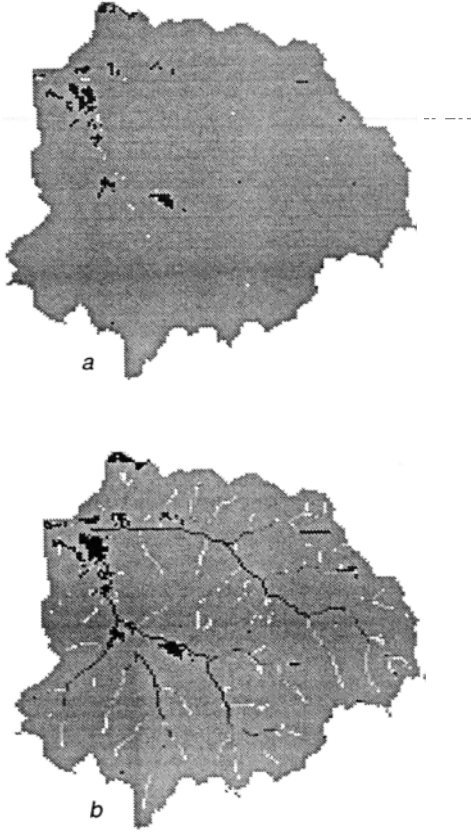
Figure 5. Modeled locations and rates of runoff generation for the King's Creek catchment on August 13, 1987, at (a) 0145 UT and (b) 0215 UT. The scale black to white represents runoff generation rates from 30 mm/h to near 0 mm/h. Medium grey background represents the remaining catchment grid elements where no surface runoff was generated. Scale is given in Figure 4.

tion capacities with continued intense precipitation. In general, runoff generation occurs in the wetter catchment grid elements, which are located adjacent to the stream network. These are locations of low infiltration capacity. Within each of Figures 5a and 5b, the magnitude of surface runoff rates increases with increasing root zone soil moisture, increasing precipitation intensity, and decreasing infiltration capacity.

3.2. Spatial Variability and the Macroscale Fluxes

3.2.1. Macroscale evapotranspiration rates. The expected macroscale evapotranspiration rate can be rewritten as

$$E[E] = e_{wc} + E[E_{dc}] + E[E_{bs}] \qquad (44)$$

where $E[E_{dc}]$ is the expected dry-canopy transpiration rate, $E[E_{bs}]$ is the expected bare-soil evaporation rate,

$$E[E_{dc}] = f_v \omega_{dc} \left[t_{unst} \int_{x=x^{sat}}^{x=\infty} f_x(x) \; dx \right.$$

$$\left. + t_{unst} \int_{x=-\infty}^{x=x^{sat}} \zeta_{vx} f_x(x) \; dx + \int_{x=-\infty}^{x=x^{sat}} \xi_{vx} \tau_x^* f_x(x) \; dx \right]$$

(45a)

with

$$\zeta_{vx} = 1 \qquad \tau_x^* \geq t_{unst} \qquad (45b)$$

$$\zeta_{vx} = 0 \qquad \tau_x^* < t_{unst} \qquad (45c)$$

$$\xi_{vx} = 1 \qquad \tau_x^* < t_{unst} \qquad (45d)$$

$$\xi_{vx} = 0 \qquad \tau_x^* \geq t_{unst} \qquad (45e)$$

$$E[E_{bs}] = f_{bs} \left[e_{pe} \int_{x=x^{sat}}^{x=\infty} f_x(x) \; dx + e_{pe} \int_{x=-\infty}^{x=x^{sat}} \zeta_{sx} f_x(x) \; dx \right.$$

$$\left. + \int_{x=-\infty}^{x=x^{sat}} \xi_{sx} e_x^*(E_c) f_x(x) \; dx \right] \qquad (46a)$$

with

$$\zeta_{sx} = 1 \qquad e_x^*(E_c) \geq e_{pe} \qquad (46b)$$

$$\zeta_{sx} = 0 \qquad e_x^*(E_c) < e_{pe} \qquad (46c)$$

$$\xi_{sx} = 1 \qquad e_x^*(E_c) < e_{pe} \qquad (46d)$$

$$\xi_{sx} = 0 \qquad e_x^*(E_c) \geq e_{pe}. \qquad (46e)$$

Simplifying the notation above, the integral $\int_{x=x^{sat}}^{x=\infty} f_x(x) \; dx$ in (45a) and (46a) represents the areal fraction of saturated land surface, and is replaced by A_{sat}/A. The second integral terms in (45a) and (46a) represent the areal fractions of vegetated and bare soil land surface that are unsaturated, but still able to supply moisture to the atmosphere at potential rates. These integrals are replaced by A_{t1}/A and A_{t2}/A, respectively, where

$$\frac{A_{t1}}{A} = \int_{x=-\infty}^{x=x^{sat}} \zeta_{vx} f_x(x) \; dx \qquad \frac{A_{t2}}{A} = \int_{x=-\infty}^{x=x^{sat}} \zeta_{sx} f_x(x) \; dx$$

(47)

The subscript t above implies that these are areas of "transition," from saturated surface areas evaporating at potential rates, to drier land surface areas outside of the transitional regions where evapotranspiration is restricted by active vegetation and soil control. The third terms in (45a) and (46a) represent the contributions to the macroscale dry-canopy and bare-soil fluxes from these areas where vegetation and soil controls on evapotranspiration are active. Defining $\bar{\tau}^* = \int_{x=-\infty}^{x=x^{sat}} \xi_{vx} \tau_x^* f_x(x) \; dx$ and $\bar{e}^* = \int_{x=-\infty}^{x=x^{sat}} \xi_{sx} e_x^*(E_c) f_x(x) \; dx$, then (45a) and (46a) can be rewritten as

$$E[E_{dc}] = \frac{A_{sat}}{A} t_{unst} + \frac{A_{t2}}{A} t_{unst} + \bar{\tau}^* \qquad (48)$$

$$E[E_{bs}] = \frac{A_{sat}}{A} e_{pe} + \frac{A_{t1}}{A} e_{pe} + \bar{e}^* \qquad (49)$$

Comparison of (48) and (49) to (39) and (40) shows that the macroscale formulation, although simplified, captures the fundamental dynamics of land-atmosphere interaction as represented by the spatially distributed formulation. Macroscale equations (48) and (49) both contain terms representing an areal fraction of saturated land surface where evapotranspiration is generated at potential rates. Both macroscale equations include terms representing the more dynamic
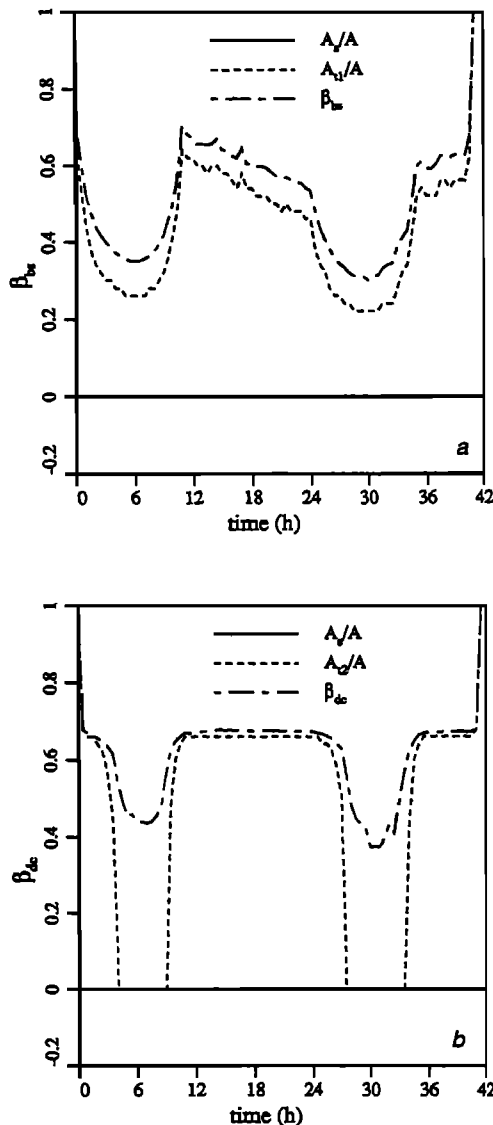
Figure 6. Modeled evaporation and transpiration efficiencies for the King's Creek Catchment, October 7–8, 1987. Time step 0 represents 1315 UT on October 7. (a) Evaporation efficiency. (b) Transpiration efficiency.

transitional regions, where evapotranspiration is also generated at potential rates. Finally, both equations represent the contribution to the macroscale flux by the areal fractions of drier land surface, where vegetation and soil controls actively limit evapotranspiration rates.

Normalizing (48) and (49) by t_{unst} and e_{pe}, respectively, yields the transpiration efficiency β_{dc}, and the evaporation efficiency β_{bs}. The efficiencies are therefore composed of three terms representing the areal fraction of saturated land surface, the transitional areal fraction, and a vegetation- or soil control term. Figure 6 shows the simulated diurnal dynamics of the efficiencies, including their various components. These efficiencies were extracted from a 12-day simulation of the King's Creek catchment (October 5–16, 1987) using the macroscale model with half-hourly time steps. Since the purpose of this section is once again demonstrative, the details of the simulation are found in the application paper [*Famiglietti and Wood*, this issue]. The

diurnal cycles shown here represent October 7 and 8, 1987, where time step 0 in Figure 6 corresponds to 1315 (UT). Figure 6 (top) shows that the components of the macroscale evaporation efficiency exhibit the diurnal dynamics described previously for the more detailed spatially distributed formulation (see Figure 4). Comparison of Figure 6 (top) to a similar plot for the spatially distributed simulation shows close agreement (not shown, but explained in the companion paper [*Famiglietti and Wood*, this issue]). The saturated area term remains constant at zero for the simulation because the King's Creek streambed was dry during this time period. The transitional area term A_{t1}/A displays the diurnal variation outlined previously. Analysis of the first 5 days of the simulation (not shown) shows that with each day, more of the bare-soil land surface falls under soil-controlled evaporation at midday. This is reflected in the evaporation efficiency in Figure 6 (top), which indicates that by October 8, actual evaporation at midday has fallen to roughly 30% of the potential rate. Figure 6 (bottom) shows the simulated transpiration efficiency and its components. The saturated area term remains constant at zero. The transitional area term falls from high levels when the unstressed transpiration is low, to zero at midday, when the entire region transpires at vegetation-controlled rates. This is consistent with the observed state of the vegetation for this time of year: the drier root zone moisture conditions lead to prolonged stress and ultimate senescence of the native tallgrass. The transpiration efficiency shows that at midday, the entire modeled region is contributing transpiration at a rate that is less than half of the unstressed rate.

Although the macroscale formulation captures some fundamental dynamics of evapotranspiration processes, it is important to note the differences between macroscale equations (44), (48), and (49), and catchment-scale equations (38)–(40). There are two major differences between the formulations, which result from the simplifying assumptions required to develop a macroscale parameterization appropriate for use in atmospheric models. First, in the spatially distributed catchment-scale equations, all model parameters and inputs are allowed to vary spatially. In the macroscale formulation, atmospheric forcing and the vegetation and soil parameters listed in Table 1 are held at areally averaged values. Therefore the difference between evapotranspiration computed with the macroscale and spatially distributed formulations will depend in part upon the degree of spatial variability present in the various model parameters and inputs, as well as the nonlinearities associated with the process equations which utilize those parameters. The second difference is that spatial variability in the macroscale formulation is represented statistically rather than in a grid-based manner. Exact patterns of the topographic-soil index and root zone moisture content are characterized by a distribution function. The bias induced by these simplifying assumptions is investigated by *Framiglietti and Wood* [this issue] and paper 3 using observed data at the King's Creek catchment.

3.2.2. Macroscale runoff rates. Since infiltration excess and saturation excess runoff are the predominant runoff generation mechanisms in many parts of the world, their inclusion in macroscale hydrological models is important for realistic large-scale runoff modeling. Although the simplifying assumptions of the macroscale model formulation result in a more restrictive representation of land surface hetero-

geneity, as is shown below, the fundamental dynamics of runoff generation are fairly well represented.

The expected runoff rate for the macroscale formulation can be expressed as

$$E[Q] = E[Q_{bs}] + E[Q_v] + \bar{Q}_{bs} \tag{50}$$

where $E[Q_{bs}]$ is the expected macroscale bare-soil runoff rate and $E[Q_v]$ is the expected runoff rate for vegetated soils,

$$E[Q_{bs}] = f_{bs}\left[p \int_{x=x^{sat}}^{x=\infty} f_x(x) \, dx \right.$$

$$\left. + \int_{x=-\infty}^{x=x^{sat}} \nu_{sx}(p - i_x^*(I)) f_x(x) \, dx \right] \tag{51a}$$

with

$$\nu_{sx} = 1 \qquad p > i_x^*(I) \tag{51b}$$

$$\nu_{sx} = 0 \qquad p \le i_x^*(I) \tag{51c}$$

$$E[Q_v] = p_{net} \int_{x=x^{sat}}^{x=\infty} f_x(x) \, dx$$

$$+ \int_{x=-\infty}^{x=x^{sat}} \nu_{vx}(p_{net} - i_x^*(I)) f_x(x) \, dx \tag{52a}$$

with

$$\nu_{vx} = 1 \qquad p_{net} > i_x^*(I) \tag{52b}$$

$$\nu_{vx} = 0 \qquad p_{net} \le i_x^*(I) \tag{52c}$$

Simplifying (51a) and (52a), the integrals $\int_{x=x^{sat}}^{x=\infty} f_x(x) \, dx$ are once again replaced by A_{sat}/A. The second integral terms in (51a) and (52a) represent the contribution to macroscale fluxes by the infiltration excess runoff mechanism. The areal fractions of bare and vegetated land surface over which infiltration excess runoff occurs are denoted A_{t3}/A and A_{t4}/A, where

$$\frac{A_{t3}}{A} = \int_{x=-\infty}^{x=x^{sat}} \nu_{sx} f_x(x) \, dx \qquad \frac{A_{t4}}{A} = \int_{x=-\infty}^{x=x^{sat}} \nu_{vx} f_x(x) \, dx \tag{53}$$

The corresponding macroscale infiltration capacities are defined as $\bar{i}_{bs}^* = \int_{x=-\infty}^{x=x^{sat}} \nu_{sx} i_x^*(I) f_x(x) \, dx$ and $\bar{i}_v^* = \int_{x=-\infty}^{x=x^{sat}} \nu_{vx} i_x^*(I) f_x(x) \, dx$, so that (51a) and (52a) can be rewritten as

$$E[Q_{bs}] = f_{bs}\left[\frac{A_{sat}}{A} p + \frac{A_{t3}}{A} p - \bar{i}_{bs}^* \right] \tag{54}$$

$$E[Q_v] = f_v\left[\frac{A_{sat}}{A} p_{net} + \frac{A_{t4}}{A} p_{net} - \bar{i}_v^* \right] \tag{55}$$

Comparing (54) and (55) with (42) and (43) shows that, in fact, runoff generation processes are well represented in the macroscale formulation. The first terms in both (54) and (55) represent the transformation of rainfall into saturation excess runoff over the areal fraction of saturated land surface. The second and third terms in the macroscale equations represent infiltration excess runoff generated over the areal
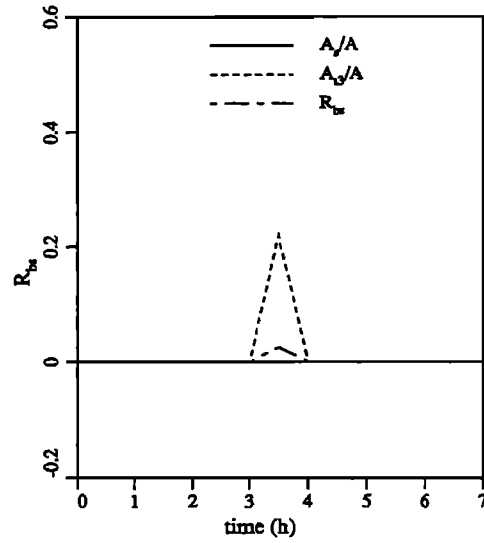

Figure 7. Modeled bare-soil runoff ratio for the King's Creek Catchment, August 12–13, 1987. Time step 0 represents 2245 UT on August 12.

fraction of unsaturated land surface where precipitation rates exceed infiltration capacities. To demonstrate how the time dynamics of runoff generation processes are represented by the macroscale formulation, the bare-soil runoff ratio R_{bs}, or $E[Q_{bs}]/p$, was simulated for the storm event described previously. Time step 0 in Figure 7 corresponds to 2245 UT and 1745 LT. The behavior of R_{bs} is consistent with the dynamics of runoff processes represented by the spatially distributed formulation. The saturated area term remains constant at zero, which is in agreement with the observed dry streambed. The transitional area term rises to nearly 0.20 after 3.5 hours, which indicates that infiltration excess runoff is generated on nearly 20% of the modeled region for the time step. The simulated runoff ratio shows that the magnitude of this infiltration excess runoff flux was small compared with the rainfall, as only 1 or 2% of the rainfall did not infiltrate.

Although (51a) and (52a) represent the predominant mechanisms of runoff generation, important differences between the macroscale and spatially distributed runoff formulations result from the different approaches to representing spatial variability. These differences were discussed in the evapotranspiration section. For example, comparison of Figure 7 to a similar plot for the spatially distributed simulation (not shown) shows that the macroscale simulation only produced runoff during one storm time step, as compared to two for the spatially distributed simulation (see Figure 5). This is primarily a result of forcing the macroscale simulation with areally averaged precipitation, thus smoothing out more intense local precipitation rates captured by the spatially distributed formulation. An approach to combat the bias induced by the macroscale formulation assumptions is described below for larger-scale applications.

4. Discussion

On the basis of our assumptions that the local and spatially distributed, catchment-scale formulations provide reasonable representations of land surface-atmosphere interaction,

this discussion focuses on applications of the macroscale formulation within atmospheric models. Model shortcomings and how to avoid them are discussed, as are model strengths, with implications for the parameterization of hydrological processes within atmospheric models.

The macroscale and spatially distributed formulations will likely diverge in their flux predictions as the scale of application increases (e.g., from mesoscale to GCM grid scales). Increasing spatial variability in atmospheric forcing, vegetation, and soil properties will render the macroscale assumptions too restrictive. To combat this problem, two alternatives exist to incorporate increased spatial variability into the macroscale model structure. The first alternative would allow certain soil and vegetation parameters listed in Table 1 (e.g., soil type or LAI), when directly correlated to the topographic-soil index, to vary with each interval of the distribution. This approach is effective as an idealized representation of high-frequency spatial variability in these parameters. The second option is to apply the macroscale formulation in "mosaic" mode [*Avissar and Pielke*, 1989; *Koster and Suarez*, 1992] when coupling to an atmospheric model, particularly one of lower resolution. In this implementation technique, a land surface grid square is partitioned into a number of subgrid patches based on major vegetation types. Climatic forcing may also be redistributed over the subgrid patches [*Seth et al.*, 1994]. Applying the macroscale formulation in mosaic mode would yield spatial variability in atmospheric forcing and major vegetation types, and within each patch, spatial variability in the topographic-soil index, root zone moisture content, and the water and energy fluxes. The simple structure of the macroscale formulation is such that it should pose no greater computational burden than other land parameterizations implemented in the same manner. The current trend toward higher-resolution atmospheric modeling, particularly in mesoscale and regional models, may render the patch solution unnecessary.

While a number of research groups are adopting the mosaic approach for representing subgrid-scale spatial variability in vegetation and soils only, it is our belief that lateral redistribution of surface and subsurface soil water is a critical control on both runoff production and energy balance and should also be incorporated in macroscale models. The macroscale formulation shows that downslope redistribution of soil water yields spatial variability in root zone moisture content, which causes the different regions of land surface outlined above to contribute runoff and evapotranspiration at different rates. Saturated areas contribute runoff and evapotranspiration at maximum rates. Transitional areas contribute evapotranspiration at maximum rates and infiltration excess runoff at lower rates which are nonlinearly related to surface moisture content. Relatively dry areas contribute no runoff and contribute evapotranspiration at lower soil- and vegetation-controlled rates, which are also nonlinearly related to surface moisture content. The temporal dynamics of these regions and the nonlinearities mentioned above suggest that lateral soil water redistribution and the resulting subgrid-scale variability in surface moisture content should be included in macroscale hydrologic parameterizations for realistic modeling of grid-scale runoff and energy fluxes.

5. Summary

An approach to modeling water and energy balance processes at local, catchment, and macroscales is presented. The approach involves aggregating well-known local process physics across scales using a topographic framework. A local SVATS is briefly described. The SVATS couples simple representations of atmospheric forcing, vertical soil moisture transport, and plant control of transpiration to compute the diurnal dynamics of land surface water balance, energy balance, and vertical recharge to the water table. The structure of the model is simple and computationally efficient, so that it can be applied repeatedly in space and time. The resulting model structure is detailed enough however, to represent the essential physics at the land-atmosphere interface.

At the catchment scale, a spatially distributed water and energy balance model is developed by applying the local SVATS to each grid element of a discretized catchment. Grid elements are coupled to each other using simple expressions for lateral subsurface flow. A digital elevation model is employed to represent catchment topography. Catchment discretization is based on the resolution of the DEM. Spatially distributed fields of model parameters and inputs (e.g., atmospheric forcing, topographic, soil, and vegetation properties) are coregistered with the DEM so that spatial variability in model outputs (e.g., soil moisture, evapotranspiration, and runoff) is represented explicitly. The catchment-average hydrologic response is the average of the local grid element responses.

A statistical-dynamical approach is utilized to simplify the large-scale modeling problem and to aggregate the SVATS to the macroscale. Spatial variability in the dominant controls on the water and energy balance is represented using a statistical distribution function. Because of our interest in improving the macroscale representation of both runoff and energy balance processes, the dominant control on hydrologic response is assumed to be the space-time distribution of surface soil moisture. This distribution is modeled by coupling the SVATS to the statistical distribution of the topographic-soil index. Therefore another assumption at this scale is that a spatially distributed representation of important process controls can be replaced by a simpler, statistical representation. The distribution of the index is discretized into a number of intervals and the local SVATS is applied at each interval. The intervals are coupled using simple expressions for lateral subsurface flow. The macroscale hydrologic fluxes are determined by aggregating local fluxes with respect to the statistical distribution of the topographic-soil index. The resulting macroscale model is called TOPLATS, and is proposed for use in atmospheric models as a grid-scale land hydrology parameterization. TOPLATS extends a successful runoff parameterization for simulation of large-scale land surface-atmosphere interaction. It incorporates subgrid-scale spatial variability in topography and soils to model downslope redistribution of soil water, which feeds back through the model structure to yield subgrid variability in water table depth, soil water storage, root zone soil moisture content, and the runoff and energy fluxes.

The spatially distributed model formulation is explored to understand the role of spatial variability in determining areal-average fluxes and the dynamics of hydrological processes. The well-known distinction between saturation ex-

cess runoff, which occurs on saturated land surface, and infiltration excess runoff, which may occur on unsaturated land surface, is well represented in the model. However, it is shown that analogous regions of hydrologic response exist for evapotranspiration processes. Saturated and transitional areas contribute evapotranspiration at potential rates. Relatively dry areas contribute evapotranspiration at lower, soil- and vegetation-controlled rates, which are nonlinearly related to surface moisture content. The temporal dynamics of these regions are explored through simulation of a diurnal evapotranspiration cycle using data from FIFE.

The macroscale formulation is analyzed and shown to represent these dynamics fairly well. It is shown that topographic redistribution of soil water and the resulting spatial variability in root zone moisture content may result in significant areal fractions of land surface where the evapotranspiration-runoff relationships exhibit nonlinearities. It is therefore suggested that these processes warrant subgrid-scale representation in land surface hydrology parameterizations for atmospheric models. When coupled to an atmospheric model, the macroscale formulation can be implemented in mosaic mode to overcome the simplifying macroscale assumptions of spatially uniform vegetation and atmospheric forcing.

References

Avissar, R., and R. A. Pielke, A parameterization of heterogeneous land-surface for atmospheric numerical models and its impact on regional meteorology, *Mon. Weather Rev.*, *117*, 2113–2136, 1989.

Avissar, R., and M. M. Verstraete, The representation of continental surface processes in atmospheric models, *Rev. Geophys.*, *28*, 35–52, 1990.

Beven, K., Runoff production and flood frequency in catchments of order *n*: An alternative approach, in *Scale Problems in Hydrology*, edited by V. K. Gupta et al., pp. 107–131, D. Reidel, Norwell, Mass., 1986.

Beven, K. J., and M. J. Kirkby, A physically based, variable contributing area model of basin hydrology, *Hydrol. Sci. Bull.*, *24*, 43–69, 1979.

Brooks, R. H., and A. T. Corey, Hydraulic properties of porous media, *Hydrol. Pap. 3*, Colo. State Univ., Fort Collins, 1964.

Deardorff, J. W., Efficient prediction of ground surface temperature and moisture, with inclusion of a layer of vegetation, *J. Geophys. Res.*, *83*, 1889–1903, 1978.

Dickinson, R. E., Modelling evapotranspiration for three-dimensional global climate models, in *Climate Processes and Climate Sensitivity, Geophys. Monogr. Ser.*, vol. 29, edited by J. E. Hansen and T. Takahashi, pp. 58–72, AGU, Washington, D. C., 1984.

Dickinson, R. E., A. Henderson-Sellers, and P. J. Kennedy, Biosphere-Atmosphere Transfer Scheme (BATS) Version 1e as coupled to the NCAR Community Climate Model, *Tech. Note TN-387+STR*, Natl. Cent. for Atmos. Res., Boulder, Colo., 1993.

Eagleson, P. S., Climate, soil and vegetation, 3, A simplified model of soil moisture movement in the liquid phase, *Water Resour. Res.*, *14*, 722–730, 1978.

Entekhabi, D., and P. S. Eagleson, Land surface hydrology parameterization for atmospheric general circulation models including subgrid scale spatial variability, *J. Clim.*, *2*, 816–831, 1989.

Famiglietti, J. S., Aggregation and scaling of spatially-variable hydrological processes: Local, catchment-scale and macroscale models of water and energy balance, Ph.D. dissertation, Princeton Univ., Princeton, N. J., 1992.

Famiglietti, J. S., and E. F. Wood, Comparison of passive microwave and model derived estimates for soil moisture fields, paper presented at the 5th International Colloquium—Physical Measurements and Signatures in Remote Sensing, Eur. Space Agency, Courcheval, France, 1991a.

Famiglietti, J. S., and E. F. Wood, Evapotranspiration and runoff from large land areas: Land surface hydrology for atmospheric general circulation models, *Surv. Geophys.*, *12*, 179–204, 1991b.

Famiglietti, J. S., and E. F. Wood, Application of multiscale water and energy balance models on a tallgrass prairie, *Water Resour. Res.*, this issue.

Famiglietti, J. S., and E. F. Wood, Effects of spatial variability and scale on areally averaged evapotranspiration, *Water Resour. Res.*, in press, 1994.

Famiglietti, J. S., E. F. Wood, M. Sivapalan, and D. J. Thongs, A catchment scale water balance model for FIFE, *J. Geophys. Res.*, *97*(D17), 18,997–19,007, 1992.

Feyen, J., C. Belmans, and D. Hillel, Comparison between measured and simulated plant water potential during soil water extraction by potted ryegrass, *Soil Sci.*, *129*, 180–185, 1980.

Gardner, W. R., Some steady-state solutions of the unsaturated moisture flow equation with application to evaporation from a water table, *Soil Sci.*, *85*, 228–239, 1958.

Koster, R. D., and M. J. Suarez, Modeling the land surface boundary in climate models as a composite of independent vegetation stands, *J. Geophys. Res.*, *97*, 2697–2715, 1992.

Liang, X., D. P. Lettenmaier, E. F. Wood, and S. J. Burges, A simple hydrologically based model of land surface water and energy fluxes for GCMs, *J. Geophys. Res.*, *99*(D7), 14,415–14,428, 1994.

McCumber, M. C., and R. A. Pielke, Simulation of the effects of surface fluxes of heat and moisture in a mesoscale numerical model, 1, Soil layer, *J. Geophys. Res.*, *86*, 9929–9938, 1981.

Milly, P. C. D., An event-based simulation model of moisture and energy fluxes at a bare soil surface, *Water Resour. Res.*, *22*, 1680–1692, 1986.

Milly, P. C. D., A refinement of the combination equations for evaporation, *Surv. Geophys.*, *12*, 145–154, 1991.

Mintz, Y., The sensitivity of numerically simulated climates to land surface conditions, in *The Global Climate*, edited by J. Houghton, pp. 79–105, Cambridge University Press, Cambridge, Mass., 1984.

Pitman, A. J., et al., Project for Intercomparison of Landsurface Parameterisation Schemes (PILPS): Results from the Off-line Control Simulations (Phase 1a), *Publ. Ser. 7*, Int. GEWEX Proj. Off. (IGPO), Washington, D.C., 1993.

Richards, L. A., Capillary conduction of liquids through porous mediums, *Physics*, *1*, 318–333, 1931.

Sellers, P. J., Y. Mintz, Y. C. Sud, and A. Dalcher, A simple biosphere model (SiB) for use within general circulation models, *J. Atmos. Sci.*, *43*, 505–531, 1986.

Sellers, P. J., F. G. Hall, G. Asrar, D. E. Strebel, and R. E. Murphy, An overview of the First International Satellite Land Surface Climatology Project (ISLSCP) Field Experiment (FIFE), *J. Geophys. Res.*, *97*(D17), 18,345–18,371, 1992.

Seth, A., F. Giorgi, and R. E. Dickinson, Simulating fluxes from heterogeneous land surfaces: An explicit subgrid method employing the Biosphere-Atmosphere Transfer Scheme (VBATS), *J. Geophys. Res.*, *99* 18,651–18, 667, 1994.

Sivapalan, M., K. Beven, and E. F. Wood, On hydrologic similarity, 2, A scaled model of storm runoff production, *Water Resour. Res.*, *23*, 2266–2278, 1987.

Wood, E. F., Global scale hydrology: Advances in land surface modeling, *Rev. Geophys.*, *29*, suppl., 193–201, 1991.

Wood, E. F., M. Sivapalan, K. Beven, and L. Band, Effects of spatial variability and scale with implications to hydrologic modeling, *J. Hydrol.*, *102*, 29–47, 1988.

Wood, E. F., M. Sivapalan, and K. Beven, Similarity and scale in catchment storm response, *Rev. Geophys.*, *28*, 1–18, 1990.

J. S. Famiglietti, Department of Geological Sciences, University of Texas at Austin, Austin, TX 78712. (e-mail:jfamiglt@maestro. geo.utexas.edu)
E. F. Wood, Water Resources Program, Department of Civil Engineering and Operations Research, Princeton University, Princeton, NJ 08544.